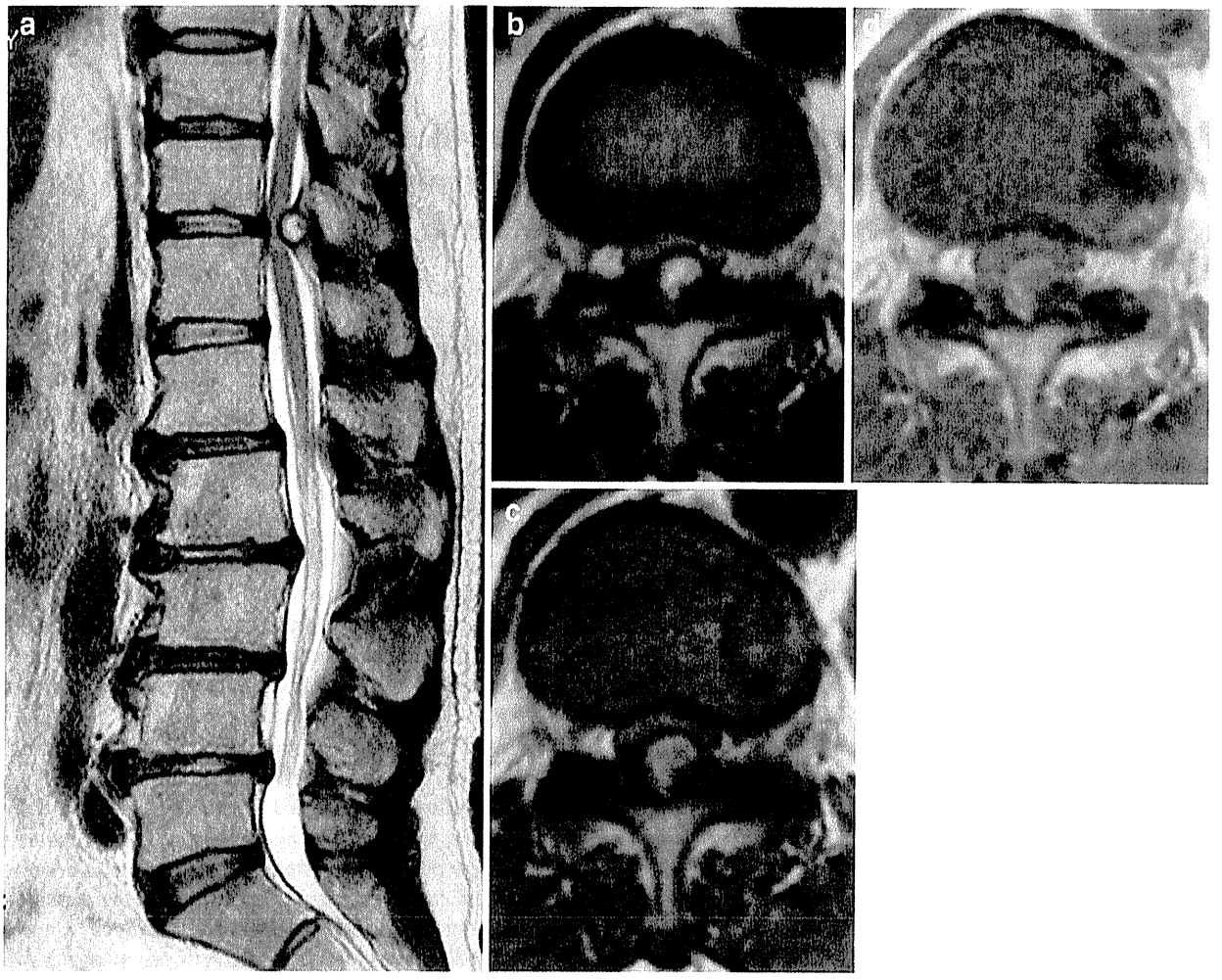

Fig. 1 Magnetic resonance imaging (MRI) showing the round mass lesion at T11–12 (**a** sagittal view, **b–d** axial view). The mass showed heterogeneous intensity with a marginally hypointense signal on the T2-weighted images (**a**, **c**) and hyperintense with a marginally hypointense signal on the T1-weighted images (**b**). The enhancement of the mass was not remarkable after intravenous administration of contrast medium (**d**)

The patient underwent partial laminectomy at T11 to T12. A solid reddish brown mass was found, firmly adhered, posteriorly to the dural sac. The mass was completely resected. Macroscopically, the resected mass showed solid and degenerative tissue with a chronic hematoma (Fig. 3). After surgery, the patient's symptoms resolved, and his gait returned to normal within 1 month. One year after surgery, neither neurological deficits nor gait disturbance was observed. The patient gave informed consent for the presentation of this case.

Patient 2

A 54-year-old man had experienced lower back pain, gait disturbance, and numbness of the lower legs for 2 months. The pain radiated into the buttocks and bilateral legs with dysesthesia. The symptoms were exacerbated by extension of the lumbar spine. On physical examination, the patient had normal muscle strength in the lower legs. The patellar tendon and Achilles tendon reflexes were not increased bilaterally. Plain radiographs of his thoracic spine showed degenerative changes at T10, T11, and T12. An MRI of the thoracic spine on the 14th day after the onset of the symptoms revealed a posterior extradural intraspinal mass at the T11/12 disc space level with substantial compression of the spinal cord. The mass was lobulated, and the proximal part of the mass showed high signal intensity in the central lesions on the T1- and T2-weighted images. On the other hand, the distal part of the mass showed high signal intensity on the T1-weighted image and low signal

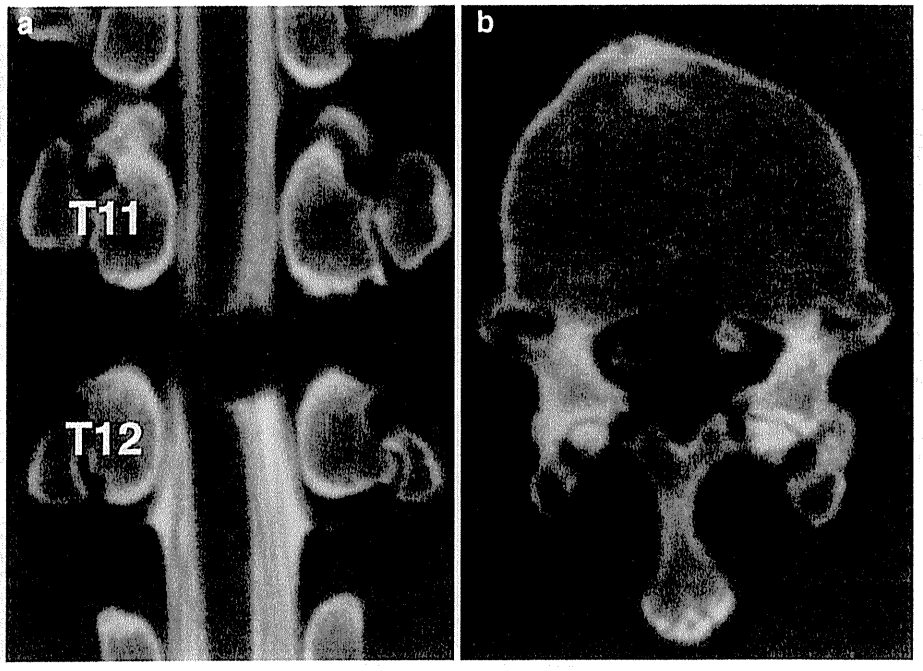

Fig. 2 Postmyelography computerized tomography (CT) indicates a large extradural lesion along with degeneration of the facet joint at the T11–12 level (**a** coronal reconstruction image, **b** axial view)

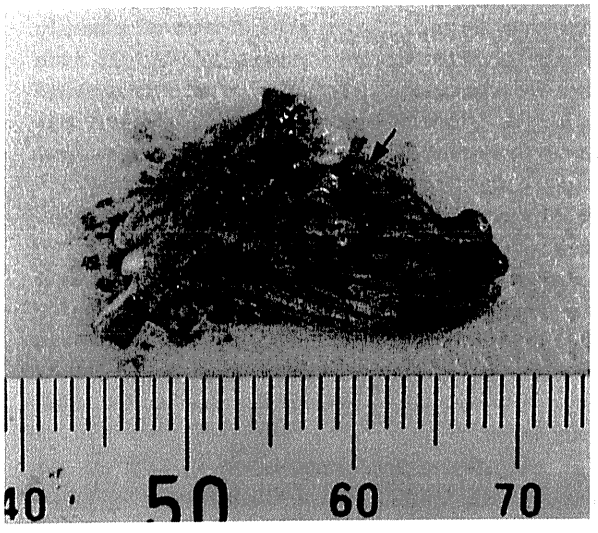

Fig. 3 Macroscopic appearance of the resected ligamentum flavum. The specimen showed a solid brownish mass with a chronic hematoma (*arrow*)

intensity on the T2-weighted images. The rim of the mass was hypointense on the T1- and T2-weighted images (Fig. 4a, b). T11 laminectomy was performed. The LF was resected, and a chronic hematoma was found in the hypertrophic and degenerative LF. Postoperatively, the patient's symptoms resolved. Seven years after surgery, the patient had no complaints. The patient gave informed consent for the presentation of this case.

Histological analysis

In patient 1, a histological examination revealed that the wall of the mass lesion was dense and composed of collagenized connective tissue. In addition, a hemorrhagic zone was also seen (Fig. 5a). There was an area in the middle of the specimen that indicated a chronic hematoma (Fig. 5b). The overall histological diagnosis was a hematoma in the degenerative LF. An immunohistochemical analysis confirmed a certain number of capillaries, as indicated by vascular endothelial cells (CD31 positive cells) (Fig. 5c). The presence of infiltrating macrophages (CD68 positive cells) in the mass was also detected (Fig. 5d). Since VEGF, a potent angiogenesis-stimulating factor, has been reported to express in degenerated LF [3], we then tested the expression of VEGF in the same specimen. Remarkably, the expression of VEGF was observed in the fibroblastic cells adjacent to the capillaries (arrows in Fig. 5e) and infiltrating macrophages (arrows in Fig. 5f). Meanwhile, TGF-beta has also been reported to express in degenerative LF [3] and to stimulate the expression of VEGF [4]. Thus, we next investigated the activation of TGF-beta signaling in the sample by using an anti-phospho-specific antibody to Smad2 (p-Smad2), a downstream signal transducer of the TGF-beta pathway [5]. Interestingly, the expression of pSmad2 was observed in the nucleus of the fibroblastic cells, and this expression pattern was similar to that of VEGF (Fig. 5g). In patient 2, histological examination revealed a hemorrhage (Fig. 6a), hemosiderin-laden macrophages (arrows in Fig. 6b), and

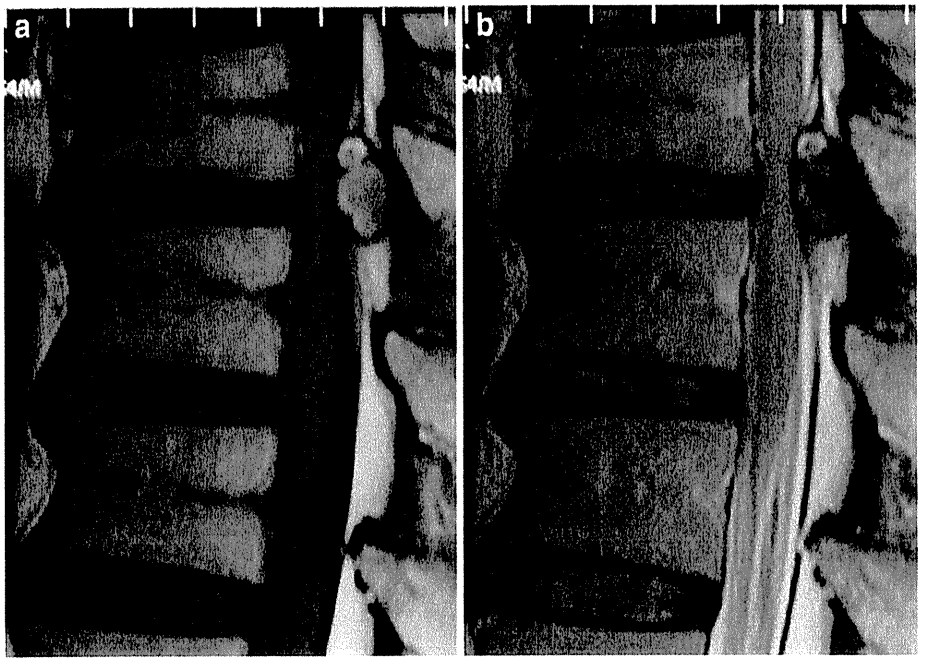

Fig. 4 MRI of the thoracic spine on the 14th day after the onset of symptoms demonstrating a posterior extradural intraspinal mass at the T11/12 disc space level with substantial compression of the spinal cord; the proximal part of the mass showed high signal intensity in the central lesions on the T1- and T2-weighted images. On the other hand, the distal part of the mass showed a high signal intensity on the T1-weighted image and low signal intensity on the T2-weighted images (**a** T1 sagittal, **b** T2 sagittal)

an increased number of capillaries (arrowheads in Fig. 6b) in the inflamed granulation tissue with elastic fibers of LF (asterisk in Fig. 6b). A degenerative change in the LF was also observed. The results of immunohistochemical analysis (CD31, CD68, VEGF, and p-Smad2) were basically the same as those observed in patient 1 (Fig. 6c–f). We then carried out the quantitative immunohistochemical analysis (CD31, CD68, VEGF, and p-Smad2) using samples of LFH ($n = 2$) and the non-degenerated LF ($n = 2$). To evaluate the number of capillaries, CD31 positive vessels were counted in five random profiles. To count the CD68, VEGF, and p-Smad2 positive cells, an image with an area of 0.64 mm^2 was settled from five random fields, and the cells were counted. The number of CD31 positive vessels was higher in the LFH compared to the non-degenerated LF (11 ± 3.7 vs. 1.1 ± 1.7). Moreover, the number of CD68, VEGF, and p-Smad2 positive cells was increased in the LFH compared to the non-degenerated LF (CD68 26.9 ± 7.7 vs. 0.4 ± 0.7; VEGF 25.5 ± 6.4 vs. 4.4 ± 2.5; p-Smad2 24.1 ± 8.7 vs. 0.8 ± 1.3) (Fig. 7a–d).

Discussion

The majority of reported cases of LFH have been seen in the mobile lumbar and cervical spine. To the best of our knowledge, only six cases of LFH in the thoracic spine, including the present cases, have been reported [2, 6–8]. According to analysis of the data obtained from these cases, an LFH in the thoracic spine revealed the following characteristic features: (1) the patients were of relatively older age (average age 62.5, range 54–72); (2) male patients were dominant (male:female = 5:1); (3) the onset of symptoms was insidious, and the clinical course progressively worsened; (4) all patients underwent surgery, and the clinical outcomes were generally favorable following surgery; (5) regarding the involved thoracic spinal segments, two cases (33%) were rigid spinal segments with the contiguous rib cage, and this level is mechanically stable. On the other hand, four cases (67%) were in the thoraco-lumbar region with its floating ribs, which are structurally and biomechanically similar to the lumbar spine, and its mobility is greater than that of the higher thoracic levels.

The pathophysiological mechanism of LFH is still unclear, but it is speculated that vessel rupture within the LF may cause the hematoma. However, the LF is poorly vascularized, and only a few small vessels pass through it, indicating that intraligamentous bleeding should be a very rare phenomenon. Meanwhile, continuous mechanical stress causes degeneration of the LF, and common pathological findings in the degenerated LF are dispersed ligamental elastic fibers, increased collagen tissues, granulation of fibrous tissues, lymphocyte infiltration, and small capillary proliferation [2, 6]. These vessels are small, thin-walled, and irregularly dispersed, and minimal and repeated spinal trauma can induce a partial tear in those vessels, causing intraligamentous hemorrhage [9]. In line with this, patient 1 had a history of mountain climbing 4 weeks before the onset of symptoms, and patient 2 had

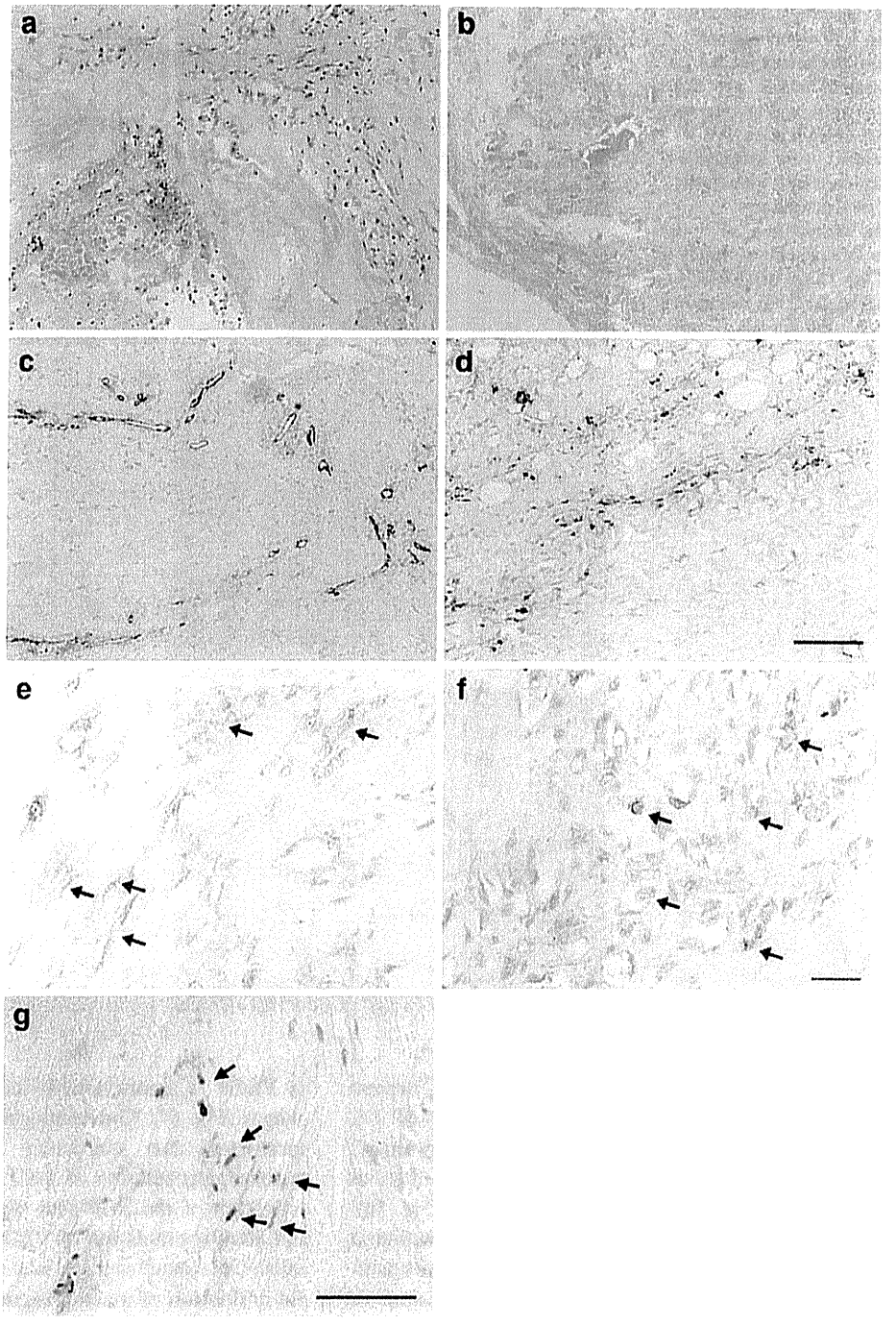

Fig. 5 Histological examination in patient 1 revealed that the wall of the mass lesion was dense and composed of collagenized connective tissue. A hemorrhagic zone was also seen (**a**). The middle of the specimen contained an area indicating a chronic hematoma (**b**) (**a**, **b**; stained with H&E). Immunohistochemical analysis confirmed a certain number of capillaries, as indicated by vascular endothelial cells (**c** CD31 positive cells). The presence of macrophages (CD68 positive cells) in the mass was also detected (**d**). The expression of VEGF was observed in the fibroblast adjacent to the capillaries (**e**), and infiltrating macrophages (**f**) were seen. The expression of phosphorylated-Smad 2 was also revealed in the fibroblastic cells (**g**). *Scale bar* 200 μm (**a**, **d**), 100 μm (**b**, **c**), 50 μm (**e**–**g**)

participated in physical labour approximately 2 months before the onset of symptoms. Once a hemorrhage occurs in the LF, along with fibrinolytic and hemolytic changes, it significantly increases in volume inside the ligament, causing neural compression. This might explain the insidious onset and progressive clinical worsening of symptoms in patients with LFH.

So what is the link between the degeneration of the LF and capillary formation in the LF? The key molecules concerning this issue are TGF-beta and VEGF. Mechanical stress has been shown to increase the production of TGF-beta in several cell lines, including ligament fibroblasts [10]. Remarkably, mechanical stretching force promotes TGF-beta production by LF cells isolated from surgically

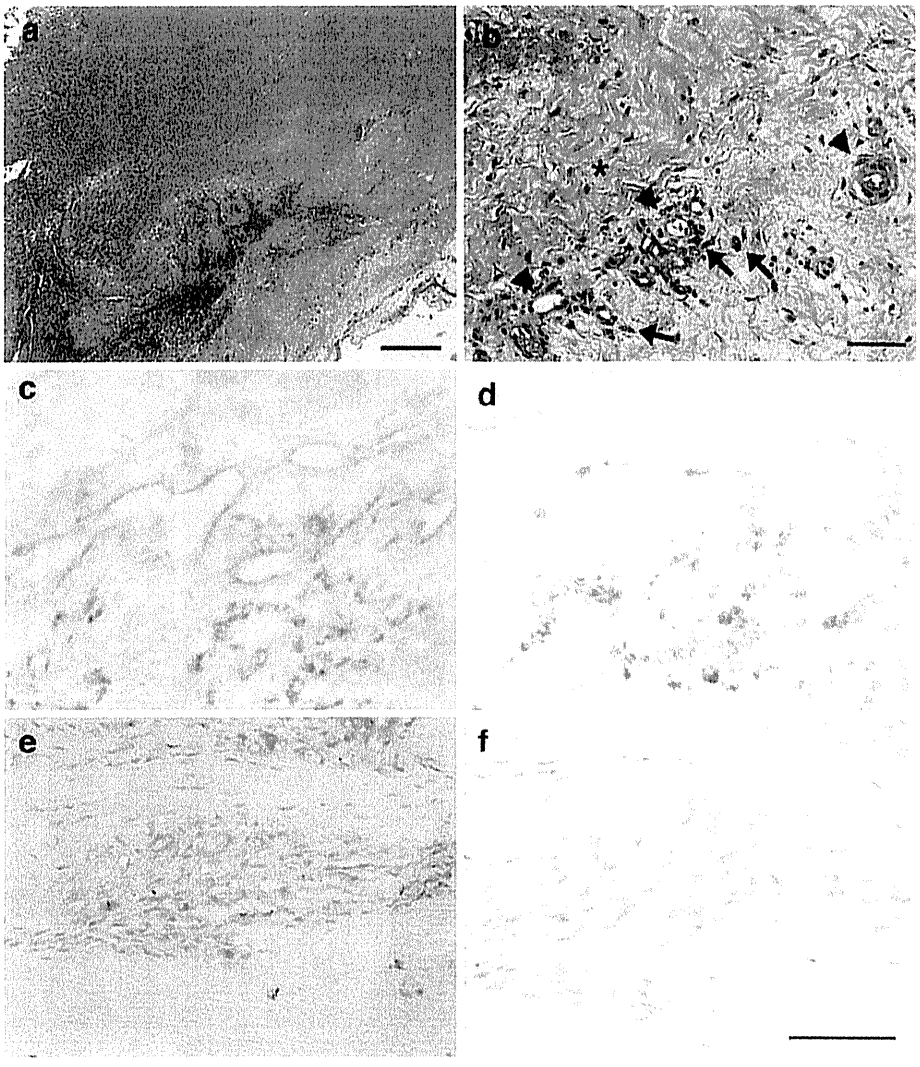

Fig. 6 Histological findings in patient 2. Photomicrographs showing the hematoma (**a**), hemosiderin-laden macrophages (*arrows* in **b**), and an increased number of capillaries (*arrow heads* in **b**) in the inflamed granulation tissue with elastic fibers of ligamentum flavum (*asterisk* in **b**). Immunohistochemical results of CD31 (**c**), CD68 (**d**), VEGF (**e**), and p-Smad2 (**f**) are also shown. *Scale bar* 200 μm (**a**), 50 μm (**b**–**d**, **f**)

resected LF [11]. In accordance with this finding, expression of TGF-beta has been reported in degenerated LF [3]. Importantly, we demonstrated the expression of p-Smad2 in the LFH specimens in the thoracic spine, indicating that TGF-beta signaling was active in our patients (Fig. 5g). TGF-beta was also found to stimulate VEGF production in fibroblasts [12]. Moreover, in cardiac myocytes, mechanical stress-induced TGF-beta stimulates expression of VEGF [13]. It has been reported that immunoreactivity to VEGF is negative in LF without degeneration [14]. In contrast, in our cases, expression of VEGF was found in the fibroblastic cells around the area of the small capillaries (Fig. 5e), suggesting that those fibroblastic cells could be a source of VEGF in degenerated LF. Since VEGF stimulates the migration of macrophages [15], VEGF in degenerated LF would also recruit macrophages, along with stimulating angiogeneis. Interestingly, we found expression of VEGF in a considerable number of infiltrating macrophages (Fig. 5f). Considering this information together, we speculated that continuous mechanical stress would increase degeneration of the LF, expression of TGF-beta, activation of the TGF-beta signaling pathway in the LF, and finally stimulation of VEGF expression in fibroblastic cells. Once small capillaries were formed, VEGF enhanced the infiltration of macrophages, and the macrophages also produced VEGF, further augmenting angiogenesis. It might be reasonable to consider this vicious circle as one of the essential pathophysiological mechanisms of LFH.

In general, the characteristic MRI findings of hematoma show a hypointense signal on the T2-weighted images at the acute stage during the first 3 days after hemorrhage because of the transition of oxygenated hemoglobin into deoxyhemoglobin, while the lesion remains isointense on the T1-weighted images. Methemoglobin in a hematoma leads to a

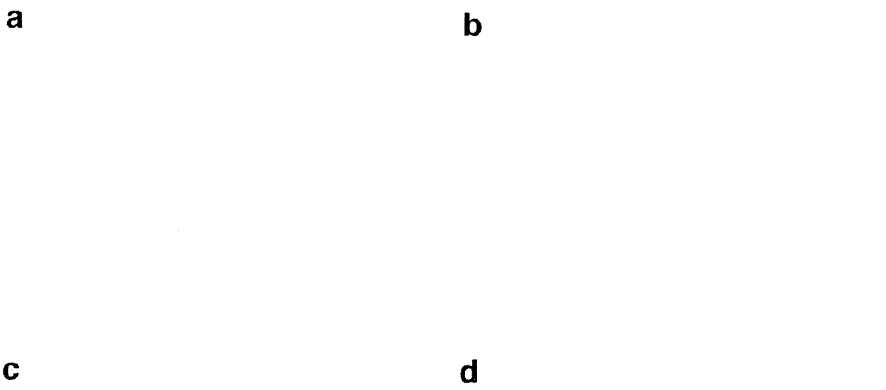

Fig. 7 Histological examination in the non-degenerated ligamentum flavum. Immunohistochemical results of CD31 (**a**), CD68 (**b**), VEGF (**c**), and p-Smad2 (**d**) are shown. *Scale bar* 50 μm

hyperintense signal on the T1-weighted images in the early subacute stage (3–7 days). Thereafter, hemolysis of the erythrocytes results in the accumulation of extracellular methemoglobin, and this is hyperintense on the T1- and T2-weighted images in the late subacute stage [16]. In patient 2, the mass was lobulated, and the proximal part of the mass showed high signal intensity on the T1- and T2-weighted images in the central lesions, revealing that the hematoma was in the late subacute stage. In contrast, the distal part of the mass showed high signal intensity on the T1-weighted image and low signal intensity on the T2-weighted images, indicating an early subacute hematoma. These findings clearly demonstrated that this LFH was caused by repeated bleeding and had a multistaged hematoma. Therefore, the MRI characteristics can give us clues to understand the clinical course of LFH and may help us determine the correct diagnosis of LFH in the thoracic spine.

Acknowledgments This paper was supported by a Grant-in-Aid for Scientific Research (C) (no. 23592192) from the Japan Society for the Promotion of Science, Tokyo, Japan.

Conflict of interest There is no conflict of interest regarding the submitted article.

References

1. Hirakawa K, Hanakita J, Suwa H, Matsuoka N, Oda M, Muro H, Fukushima T. A post-traumatic ligamentum flavum progressive hematoma. Spine. 2000;25:1182–4.
2. Maezawa Y, Baba H, Uchida K, Kokubo Y, Kubota C, Noriki S. Ligamentum flavum hematoma in the thoracic spine. Clin Imaging. 2001;25:265–7.
3. Yayama T, Uchida K, Kobayashi S, Kokubo Y, Sato R, Nakajima H, Takamura T, Bangirana A, Itoh H, Baba H. Thoracic ossification of the human ligamentum flavum: histopathological and immunohistochemical findings around the ossified lesion. J Neurosurg Spine. 2007;7:184–93.
4. Zheng W, Seftor EA, Meininger CJ, Hendrix MJ, Tomanek RJ. Mechanisms of coronary angiogenesis in response to stretch: role of VEGF and TGF-beta. Am J Physiol Heart Circ Physiol. 2001; 280:H909–17.
5. van der Kraan PM, Blaney Davidson EN, Blom A, van den Berg WB. TGF-beta signaling in chondrocyte terminal differentiation and osteoarthritis: modulation and integration of signaling pathways through receptor-Smads. Osteoarthritis Cartilage. 2009;17: 1539–45.
6. Spuck S, Stellmacher F, Wiesmann M, Kranz R. A rare case of radicular complaint ligamentum flavum hematoma. Clin Orthop Relat Res. 2006;443:337–41.
7. Sudo H, Abumi K, Ito M, Kotani Y, Takahata M, Hojo Y, Sanda M, Minami A. Spinal cord compression by ligamentum flavum hematoma in the thoracic spine. Spine. 2009;34:E942–4.
8. Lee HW, Song JH, Chang IB, Choi HC. Spontaneous ligamentum flavum hematoma in the rigid thoracic spine: a case report and review of the literature. J Korean Neurosurg Soc. 2008;44:47–51.
9. Minamide A, Yoshida M, Tamaki T, Natsumi N. Ligamentum flavum hematoma in the lumbar spine. J Orthop Sci. 1999;4: 376–9.
10. Kimoto S, Matsuzawa M, Matsubara S, Komatsu T, Uchimura N, Kawase T, Saito S. Cytokine secretion of periodontal ligament fibroblasts derived from human deciduous teeth: effect of mechanical stress on the secretion of transforming growth factor-beta 1 and macrophage colony stimulating factor. J Periodontal Res. 1999;34:235–43.
11. Nakatani T, Marui T, Hitora T, Doita M, Nishida K, Kurosaka M. Mechanical stretching force promotes collagen synthesis by

cultured cells from human ligamentum flavum via transforming growth factor-beta1. J Orthop Res. 2002;20:1380–6.
12. Pertovaara L, Kaipainen A, Mustonen T, Orpana A, Ferrara N, Saksela O, Alitalo K. Vascular endothelial growth factor is induced in response to transforming growth factor-beta in fibroblastic and epithelial cells. J Biol Chem. 1994;269:6271–4.
13. Seko Y, Seko Y, Takahashi N, Shibuya M, Yazaki Y. Pulsatile stretch stimulates vascular endothelial growth factor (VEGF) secretion by cultured rat cardiac myocytes. Biochem Biophys Res Commun. 1999;25:462–5.
14. Yayama T, Kobayashi S, Sato R, Uchida K, Kokubo Y, Nakajima H, Takaharu T, Mwaka E, Orwotho N, Baba H. Calcium pyrophosphate crystal deposition in the ligamentum flavum of degenerated lumbar spine: histopathological and immunohistological findings. Clin Rheumatol. 2008;27:597–604.
15. Matsumoto Y, Tanaka K, Hirata G, Hanada M, Matsuda S, Shuto T, Iwamoto Y. Possible involvement of the vascular endothelial growth factor-Flt-1-focal adhesion kinase pathway in chemotaxis and the cell proliferation of osteoclast precursor cells in arthritic joints. J Immunol. 2002;168:5824–31.
16. Dorsay T, Helms C. MR imaging of epidural hematoma in the lumbar spine. Skeletal Radiol. 2002;31:677–85.

Human Pathology (2011) xx, xxx–xxx

ELSEVIER

Human PATHOLOGY

www.elsevier.com/locate/humpath

Original contribution

Inhibin-α and synaptophysin immunoreactivity in synovial sarcoma with granular cell features

Nokitaka Setsu MD [a], Kenichi Kohashi MD, PhD [a], Makoto Endo MD [a], Hidetaka Yamamoto MD, PhD [a], Yoshihiro Ohishi MD, PhD [a], Kazunobu Sueyoshi MD, PhD [b], Yukihide Iwamoto MD, PhD [c], Masazumi Tsuneyoshi MD, PhD [d], Toru Motoi MD, PhD [e], Arisa Kumagai MHS, CT, MT [e], Yoshinao Oda MD, PhD [a,*]

[a]*Department of Anatomic Pathology, Graduate School of Medical Science, Kyushu University, Fukuoka 812-8582, Japan*
[b]*Department of Pathology, Kagoshima City Hospital, Kagoshima 892-8580, Japan*
[c]*Department of Orthopedics, Graduate School of Medical Science, Kyushu University, Fukuoka 812-8582, Japan*
[d]*Department of Pathology, Fukuoka Sannou Hospital, Fukuoka 814-0001, Japan*
[e]*Department of Pathology, Teikyo University School of Medicine, Tokyo 173-8605, Japan*

Received 25 April 2011; revised 13 July 2011; accepted 21 July 2011

Keywords:
Synovial sarcoma;
Unusual histology;
Granular cell features;
Inhibin;
Synaptophysin

Summary We recognized immunoreactivity for the α subset of inhibin and synaptophysin in synovial sarcomas with granular cell features. Histologic findings of 90 cases of synovial sarcoma were reviewed. Two (2.2%) of the 90 cases had granular cell features, showing sheet or nested proliferation of characteristic epithelioid cells with abundant eosinophilic and granular cytoplasm, in addition to the typical spindle cell component. The 2 cases were both female (aged 86 and 76 years). The tumors were located in the foot and the retroperitoneum and measured 3.5 and 14 cm in maximum diameter. Reverse transcriptase polymerase chain reaction analysis revealed *SS18-SSX1* transcripts in both cases. *SS18* gene rearrangement was detected in granular cells as well as spindle cells by chromogenic in situ hybridization. Immunohistochemistry found the granular cells to be positive for inhibin-α in both cases and for synaptophysin in 1 case, whereas spindle cells were not. Thirty-six cases (20 monophasic fibrous, 11 biphasic, and 5 poorly differentiated synovial sarcomas) were additionally examined for comparison; they showed no immunoreactivity for inhibin-α or synaptophysin. This is the first report of immunoreactivity for inhibin-α and synaptophysin in synovial sarcoma. These immunohistochemical findings might be characteristic of synovial sarcomas with granular cell features.
© 2011 Elsevier Inc. All rights reserved.

1. Introduction

Synovial sarcoma (SS) occurs primarily in the extremities, usually close to joints, although it does not arise from or differentiate toward the synovium. SS can also occur away from the extremities, such as in the lung, the head and neck, or the abdominal wall. Rare anatomical sites including intra-

* Corresponding author. Department of Anatomic Pathology, Pathological Sciences, Graduate School of Medical Sciences, Kyushu University, Maidashi 3-1-1, Higashi-ku, Fukuoka 812-8582, Japan.
E-mail address: oda@surgpath.med.kyushu-u.ac.jp (Y. Oda).

0046-8177/$ – see front matter © 2011 Elsevier Inc. All rights reserved.
doi:10.1016/j.humpath.2011.07.012

abdominal or retroperitoneal regions such as the kidney [1-3], prostate [4], fallopian tube [5], and vulva [6] have been reported. Some earlier studies have reported a series of intra-abdominal or retroperitoneal cases [7,8].

Histologically, there are 2 major subtypes of SS: biphasic SS and monophasic SS. Biphasic SS has both spindle cell and epithelial components in various proportions. The tumor cells in the epithelial component form a glandular structure and sometimes look papillary. In some poorly differentiated SSs, large epithelioid cells proliferate in sheets, but they usually have clear cytoplasms.

In this study, we report 2 cases of SS arising in the foot and the retroperitoneum, which demonstrated a distinct epithelioid component with a granular cell feature in addition to the typical spindle cell component, arising in a series of 90 cases of SS. In the diagnosis of the retroperitoneal case, its location and peculiar histologic features needed immunohistochemistry with a wide spectrum of antibodies. An immunohistochemical feature that seemed unusual for SS was positivity for inhibin-α, synaptophysin, and Wilms tumor protein 1 (WT1), and therefore, we compare the immunohistochemical expression of these proteins in granular SS cases and 36 cases of conventional SS.

2. Materials and methods

2.1. Patients and materials

Two tumors with similar histologic features were identified in 90 reviewed cases of SS. All cases were registered in the Department of Anatomic Pathology, Graduate School of Medical Sciences, Kyushu University, Japan, between 1980 and 2010. The remaining 88 cases comprised 59 monophasic fibrous, 23 biphasic, and 6 poorly differentiated SSs [9].

For immunohistochemistry, formalin-fixed and paraffin-embedded samples were obtained from these 2 cases with granular cell features and 36 control cases among the total of 90 cases. The control cases consisted of 20 monophasic fibrous, 11 biphasic, and 5 poorly differentiated SSs. A fresh-frozen sample obtained from case 1 and formalin-fixed, paraffin-embedded tissue from case 2 were used for reverse transcriptase polymerase chain reaction (RT-PCR) to detect *SS18-SSX* fusion transcripts. The institutional review board at Kyushu University approved this study (permission code: 22-74).

2.2. Immunohistochemistry

Formalin-fixed, paraffin-embedded tissue was cut at 3 μm, mounted on slides, and dried at 58°C overnight. The primary antibodies are summarized in Table 1. Antigen retrieval was carried out by incubating the slides in 0.1% (wt/vol) trypsin or by boiling the slides with 10 mmol/L sodium citrate buffer (pH 6.0, with or without 0.1% Tween-20) or with Target Retrieval Solution (TRS; DAKO, Carpinteria, CA). The immune complex was visualized with the DAKO EnVision Detection System. Adequate positive controls were applied in each series of immunostaining, and negative controls were obtained by skipping the primary antibodies.

2.3. RT-PCR and sequence analysis

Total RNA was extracted from the frozen (case 1) and paraffin-embedded (case 2) samples using a TRIzol reagent (Invitrogen, Carlsbad, CA) and was reverse transcribed using Superscript III reverse transcriptase (Invitrogen) to prepare the first-strand complementary DNA.

An *SS18-SSX* fusion assay was based on the previously reported primers [10] that specifically amplify the fusion gene transcripts of *SS18-SSX1* and *SS18-SSX2*. Each PCR product (5 μL) was loaded onto 2% agarose gel with ethidium bromide and visualized under UV illumination. The PCR products were also evaluated by direct sequence analysis using the Big-Dye terminator method (version 1.1; Applied Biosystems, Foster City, CA) to confirm the breakpoints of fusion transcripts.

2.4. Dual-color chromogenic in situ hybridization

The rearranged *SS18* gene was detected using a dual-color chromogenic in situ hybridization (dc-CISH). Dual-color break-apart probes were designed and generated as previously reported [11,12]. The dc-CISH procedure was previously described [11]. Briefly, 3-μm-thick formalin-fixed, paraffin-embedded sections were deparaffinized, dehydrated, and air dried. After proteinase digestion for 10 minutes, hybridization was carried out using a hybridizer (DAKO). Signals were visualized by Dako DuoCISH using an automated immunostainer (Autostainer plus; DAKO). As for signal interpretation, the rearrangement of *SS18* gene was judged as definitely positive when isolated red and blue signals and a paired signal were observed in individual nuclei of tumor cells [12].

2.5. Ultrastructural evaluation

Tissue samples from the 2 cases with granular cell features were examined by electron microscopy (JEOL JEM-1011 electron microscope; JEOL, Tokyo, Japan). Formalin-fixed tumor tissues were refixed in 2% glutaraldehyde and in 1% osmium tetroxide. The refixed sections were embedded in epoxy resins and stained with toluidine blue for trimming and were confirmed to contain granular cell components. Thin sections were placed on carbon-coated copper grids for observation under the electron beam.

3. Results

3.1. Patients' characteristics

The 2 cases that histologically showed granular cell features both occurred in women. Patients 1 and 2 were 86 and 76 years

Table 1 Primary antibodies used in this study

Antigen	Clone	Source	Dilution	Antigen retrieval time
α-SMA	1A4	Sigma Chemicals, St Louis, MO	1:5000	None
β-Catenin	14/β-Catenin	BD Biosciences, Bedford, MA	1:200	Citrate buffer + Tween, 99°C, 15 min
Calretinin	Polyclonal	Invitrogen, Carlsbad, CA	1:50	Citrate buffer, 99°C, 20 min
CD10	56C6	Novocastra, Newcastle upon Tyne, UK	1:100	Citrate buffer, 99°C, 30 min
CD68	KP1	Dako Cytomation, Carpinteria, CA	1:300	Citrate buffer, 99°C, 20 min
CD99	12E7	Dako Cytomation	1:100	None
Chromogranin A	Polyclonal	Dako Cytomation	1:1500	None
CK7	OV-TL12/30	Dako Cytomation	1:50	Citrate buffer + Tween, 99°C, 20 min
CK19	RCK108	Dako Cytomation	1:50	Citrate buffer + Tween, 99°C, 20 min
EMA	E29	Dako Cytomation	1:400	None
Estrogen receptor	1D5	Dako Cytomation	1:2	TRS, 99°C, 40 min
Inhibin-α	R1	Serotec, Oxford, UK	1:100	TRS, 97°C, 40 min
Ki-67	MIB-1	Dako Cytomation	1:100	Citrate buffer + Tween, 99°C, 20 min
Lysozyme	Polyclonal	Dako Cytomation	1:500	None
Melan A	A103	Novocastra	1:25	EDTA, 99°C, 20 min
NCAM	1B6	Novocastra	1:50	Citrate buffer, 99°C, 10 min
Progesterone receptor	PgR636	Dako Cytomation	1:6	TRS, 99°C, 40 min
S100 protein	Polyclonal	Dako Cytomation	1:400	Trypsin, 37°C, 30 min
Synaptophysin	SY38	Dako Cytomation	1:50	Citrate buffer, 99°C, 20 min
TLE1	M-101	Santa Cruz Biotechnology, Santa Cruz, CA	1:40	Citrate buffer, 99°C, 20 min
WT1	WT49	Mitsubishi Chemical Medience, Tokyo, Japan	1:20	TRS, 99°C, 20 min

Abbreviation: SMA, smooth muscle actin.

old, with tumors located in the foot and the retroperitoneum and measuring 3.5 and 14 cm in maximum diameter, respectively. The patients had no relevant history. They had undergone surgical wide resection without any adjuvant therapies. Chromosomal analysis was performed in case 1 and revealed a complex karyotype including an (X;18) translocation [44, X, t (X;18) (p11.2;q11.2), der (1;11) (q10; q10), t (1;3) (q12;q27), add (18) (p11.2), −19]. Patient 1 did not show local recurrence or metastasis in 1 year after the surgery. Patient 2 showed local recurrence 2 months after the resection. The recurrent tumor increased in size despite the administration of chemotherapy and was surgically resected 9 months after the initial surgery. The recurrent tumor was 7 cm in diameter, focally involving small intestine and colon and histologically composed of spindle cell component only. Patient 2 was alive at the final follow-up, 11 months after the first operation.

The 36 control subjects on which immunohistochemical studies were performed consisted of 12 males and 24 females (mean age, 40 years; age range, 10-70 years).

3.2. Histologic examination

Cases 1 and 2 showed a typical spindle cell proliferation in fascicles but, importantly, also had sheets or nests of epithelioid cells with prominent eosinophilic granular cytoplasms (Fig. 1A-D). The 2 components showed a sharp abutment with each other. Case 1, which was initially diagnosed as monophasic fibrous SS, had a focal area (about 10% of maximal cut surface) of granular cells. The granular cell component was predominant (about 70%) in case 2. Case 2 also displayed a focal aggregate of epithelioid cells arranged in nests or strands, compatible with the typical epithelioid component of biphasic SS (Fig. 1B, inset). Tumor necrosis and hemorrhage were seen, but calcification or ossification was not observed in either case. The mitotic counts per 10 high-power fields in the spindle cell and granular cell components were 14 and 17 in case 1, and 12 and 21 in case 2, respectively. The cytoplasm of granular cells in case 1 revealed a weak positivity for periodic acid–Schiff stain and was diastase resistant, whereas the granules in case 2 were negative. Phosphotungstic acid–hematoxylin stain and Grimelius stain were negative in both cases.

3.3. Immunohistochemistry

The results of immunohistochemical study are shown in Fig. 2 and summarized in Table 2. Both cases with granular cell features displayed epithelial markers in each component (Fig. 2A). The granular cell components showed immunopositivity for inhibin-α in both cases (Fig. 2B and C) and synaptophysin (Fig. 2D) and WT1 only in case 2, whereas spindle tumor cells were negative for these antibodies. The immunohistochemical localization of inhibin-α and synaptophysin was recognized in cytoplasm, and that of WT1 was confined to the nucleus.

Thirty-six control cases were examined for immunoreactivity of inhibin-α, synaptophysin, and WT1 (Table 3). Four cases among them displayed inhibin-α–positive cells, but the staining was weak and scant (<0.01% positive cells) and, therefore, was interpreted as negative. No immunoreactive cells for synaptophysin were observed in any of the control

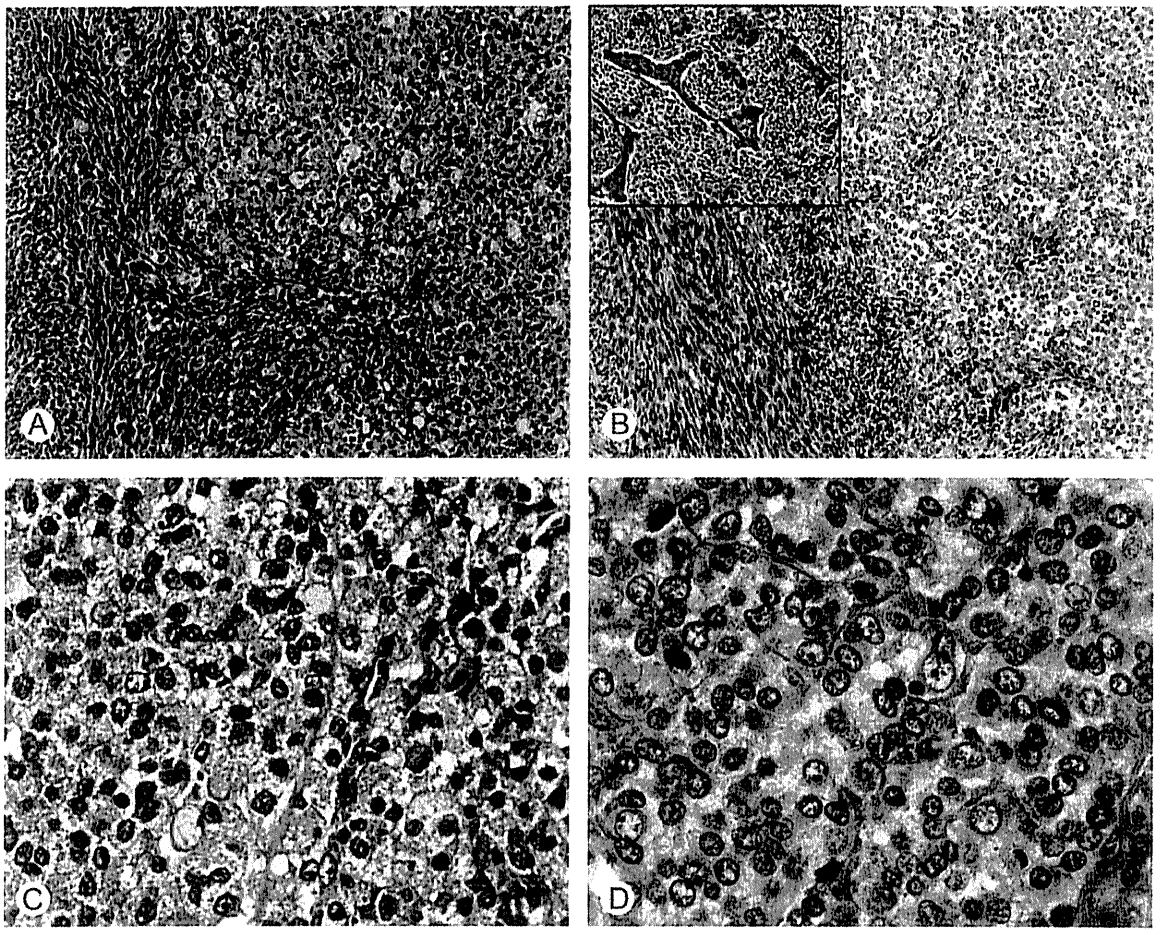

Fig. 1 SS with granular cell features. A (case 1) and B (case 2), Nests or sheets of granular epithelioid cells (right) showed a sharp abutment with the typical spindle cell component (left). A component of classical epithelioid cells arranged in strands was focally observed in case 2 (B, inset; ×100). C (case 1), The epithelioid cells had eosinophilic granular cytoplasm and showed nuclear atypia (×400). D (case 2), Tumor cells with granular cytoplasm were focally proliferated in small nests or in a cordlike pattern (×400).

cases. WT1 staining was recognized in the nuclei of spindle cells in 6 (17%) of 36 cases.

3.4. RT-PCR and sequence analysis

Both cases showed *SS18-SSX1* fusion gene transcripts by RT-PCR and after electrophoresis. The breakpoint of *SS18* and *SSX1* was confirmed by bidirectional sequencing.

3.5. Dual-color chromogenic in situ hybridization

dc-CISH enabled a simultaneous visualization of the tumor cell morphology and the gene rearrangement. The rearranged *SS18* was observed in granular cells as well as other tumor cells in each case (Fig. 3).

3.6. Ultrastructural findings

Electron microscopic analyses were completed on tissues from cases 1 and 2. Ultrastructurally, both cases showed electron-dense granules in epithelioid granular tumor cells, the size of which were 80 to 750 nm (mean, 300 nm) in case 1, and 240 to 800 nm (mean, 450 nm) in case 2. The granules were mostly round in shape and sometimes vacuolated. Especially in case 1, these granules were numerous. A few mitochondria were also observed in case 1. Case 2 showed some fine filaments suggesting tonofilaments. Dense-core granules suggesting neuroendocrine granules, neurotubules, or synaptic-like vesicles were not observed in these cases.

4. Discussion

The current study describes 2 cases of SS that had unusual histologies of epithelioid cells with granular cell features in addition to typical spindle cells (cases 1 and 2) and focal conventional epithelioid structures (case 2). The granular cells proliferated in sheets or nests, contained abundant eosinophilic and granular cytoplasm, and showed inhibin-α

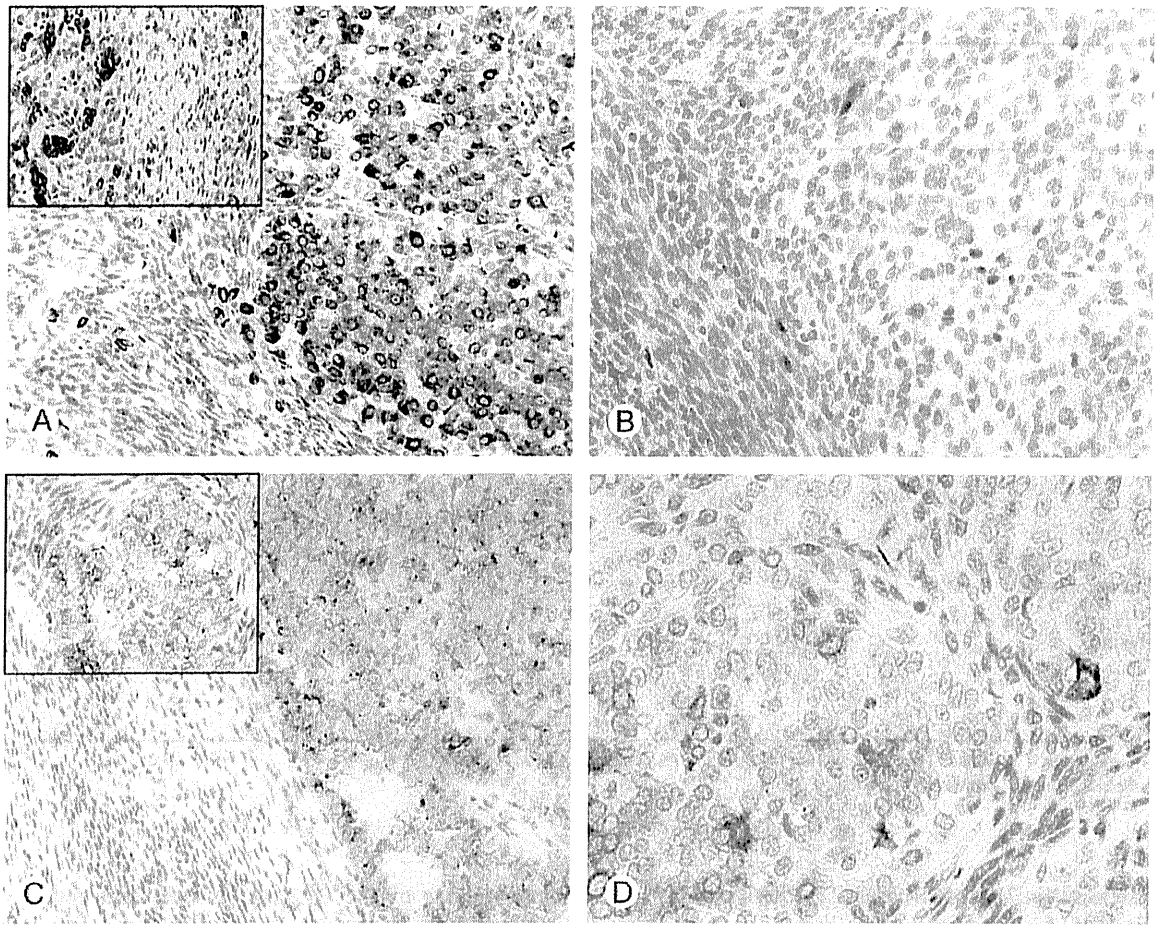

Fig. 2 Immunohistochemistry of granular SS. A (CK19, case 2), The granular epithelioid cells were positive for CK19. The strands of classical epithelioid cells was strongly positive, and spindle cells were also focally positive (inset; ×200). B (inhibin-α, case 1), Immunostaining of inhibin-α was recognized in the cytoplasm of granular cells (×200). C (inhibin-α, case 2), The granular cell component (right) was positive for inhibin-α, whereas spindle cells (left) were negative. The granular cell component with inhibin-α positivity was clearly distinguished from intermingled spindle cells (inset; ×100). D (synaptophysin, case 2), Some granular cells in case 2 were strongly positive for synaptophysin (×400).

(cases 1 and 2) and synaptophysin (case 2) immunoreactivity, which are considered unusual for SS.

SS has 2 distinct histologic components: a spindle cell component in which short spindle cells with oval nuclei proliferate in fascicles and an epithelioid component that often shows a glandular structure. SS, having both of these components, is defined as *biphasic SS*, and that with either component is diagnosed as *monophasic SS*, though a purely monophasic epithelioid SS is rare. A certain number of poorly differentiated SSs also exist, which show proliferation of epithelioid cells, small round cells, or high-grade spindle cells [13]. There are minor morphologic variants such as SS with ossification [14,15], with squamous metaplasia [16,17], and with a predominant myxoid background [18]. However, to our knowledge, only 1 article has reported SS with granular cells [16]. The authors of the article documented the detailed histologic findings of 2 cases with granular cell features in addition to other rare findings but did not describe the immunohistochemical character of the cases. Interestingly, their series of 32 SS cases were all older subjects (aged ≥60 years), similar to our 2 cases. Granular cell features of SS might be characteristic in old age.

Most cases of SS show immunoreactivity for epithelial markers: namely, cytokeratins (CKs) and epithelial membrane antigen (EMA), with a higher sensitivity for EMA. Even poorly differentiated SS cases show immunostaining of EMA and CK in 95% and 42%, respectively [19]. Among CKs, CK7 and CK19 are expressed in spindle cells of SS, in contrast to other spindle cell sarcoma [20,21]. As shown in Table 2, the present cases with granular features expressed EMA and CKs, with a higher intensity and a larger proportion in the epithelioid granular component than in spindle cell component, like most biphasic SS cases. Our cases were also positive for calretinin and neural cell adhesion molecule (NCAM). Calretinin, which is usually recognized as a mesothelioma marker, has recently been

Table 2 Immunohistochemical features of each component in granular SS cases

	Case 1		Case 2		
	Granular	Spindle	Granular	Spindle	Conventional epithelioid
α-Smooth muscle actin	−	f+	−	f+	−
β-Catenin [a]	++	+	++	+	+
Calretinin	f+	−	+	f+	−
CD10	−	−	−	−	−
CD68	−	−	−	−	−
CD99	s+	−	−	−	−
Chromogranin A	−	−	−	−	−
CK7	−	f+	f+	+	f+
CK19	−	f+	+	f+	++
EMA	s+	−	+	f+	++
Estrogen receptor	−	−	−	−	−
Inhibin-α	+	−	++	−	−
Lysozyme	−	−	−	−	−
Melan A	−	−	−	−	−
NCAM	f+−	f+	+	+	−
Progesterone receptor	−	−	−	−	−
S100 protein	−	−	−	−	−
Synaptophysin	−	−	+	−	−
TLE1	++	++	++	++	++
WT1	−	−	s+	f+	f+
Ki-67 (%)	50	50	40	30	20

++, strong; +, moderate; +−, weak; −, negative staining; f, focal (≤10% positive cells); s, scattered (≤3%)

[a] Only nuclear β-catenin expression is scored as positive.

reported in no less than 71% of SS cases [22]. Olsen et al [23] reported that NCAM-positive cells were observed in 16 of 23 SS cases. WT1 is a transcriptional regulator and a tumor suppressor that has been reported to be rarely expressed in SS, for example, in none of 60 [22] and 1 of 10 cases [24]. Case 2 showed WT1 immunoreactivity in both spindle cell and epithelioid components, but we found that WT1-positive SS was not so rare, comprising 6 (17%) of the 36 control SS cases as well. One striking immunohistochemical feature of the present cases was immunoreactivity for inhibin-α and its specificity for the epithelioid granular cell component. A previous study reported that none of 15 SS cases was positive for inhibin-α [25]. We confirmed this result by inhibin-α immunostaining of the 36 control cases and found no positive case. Moreover, case 2 showed immunopositivity for synaptophysin in the granular cell component. Olsen et al [23] found no positive case for synaptophysin in their series of 23 SS cases. None of our 36 control cases showed any immunoreactivity for synaptophysin, either. Thus, the positivity of one of our granular cases for synaptophysin constituted another specific immunohistochemical feature.

Table 3 Immunohistochemical results of control cases

	Histologic subtype			
	MSS	BSS		PDSS
		Spindle	Epithelioid	
Inhibin-α	0/20	0/11	0/11	0/5
Synaptophysin	0/20	0/11	0/11	0/5
WT1	2/20 [a]	4/11 [b]	0/11	0/5

Abbreviations: MSS, monophasic SS; BSS, biphasic SS; PDSS, poorly differentiated SS.

[a] Moderate and diffuse nuclear staining.

[b] Moderate and focal nuclear staining.

The α subset of inhibin is expressed in normal tissue such as the luminal epithelium, glands, endometrial stroma, and vascular endothelium [26]. Inhibin-α is also expressed in certain kinds of tumor and is used as an immunohistochemical diagnostic marker, though its contribution to tumorigenesis is not clearly understood. Case 2, which showed synaptophysin positivity, was negative for another neuroendocrine marker, chromogranin A. Furthermore, an ultrastructural study detected no synaptic-like vesicles in this case. Other ultrastructural findings and special stains failed to reveal the function or the significance of the granular cells.

As for histologic diagnosis of the SS cases with granular cell features, other typical components could lead to the diagnosis of SS, but a predominant granular cell component or unusual tumor location (like case 2) would mislead the diagnosis. Such cases of granular SS, especially in abdominal spaces, should be distinguished from tumors with a biphasic appearance of epithelioid and spindle cell features, such as malignant mesothelioma, carcinosarcoma,

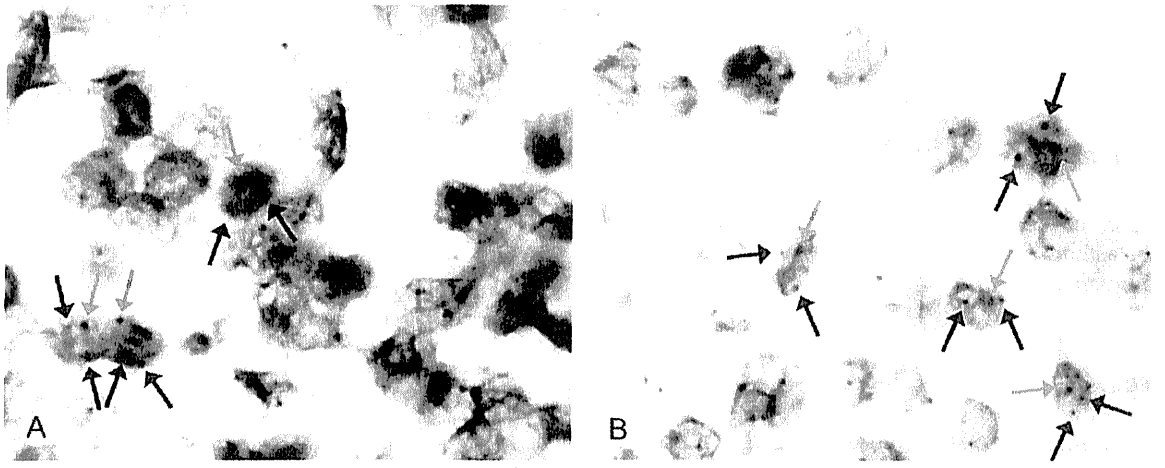

Fig. 3 dc-CISH. A (case 1) and B (case 2), Split of blue and red signals (red arrows) with a paired signal (green arrow) was observed in the nuclei of epithelioid granular cells, which indicated the presence of the rearrangement of *SS18* gene.

gastroblastoma [27], and certain types of sex cord–stromal tumors. *Biphasic malignant mesotheliomas* consist of epithelial and sarcomatous components, but they usually blend with one another, and transitional areas may be seen. Our cases of granular SS, like most biphasic SS, showed an abrupt transition of the epithelioid granular and spindle cell components. Immunohistochemically, calretinin is not useful for distinguishing malignant mesothelioma from SS as mentioned above. Matsuyama et al [28] reported that positivity of transducin-like enhancer protein 1 (TLE1), which is considered as an immunohistochemical marker of SS, is recognized in 69% of malignant mesotheliomas and is not reliable either. Immunostaining of CD10 and β-catenin might be helpful, because 37% to 54% of malignant mesotheliomas are positive for CD10 [29,30] and show no nuclear accumulation of β-catenin [28], whereas the granular SS cases were negative for CD10 and revealed β-catenin expression in the nuclei. *Carcinosarcomas* that show a high-grade appearance with highly atypical adenocarcinomatous, squamous, or undifferentiated epithelial elements differ from granular SS, in which each component shows a relatively monotonous appearance. *Gastroblastomas*, as recently reported by Miettinen et al [27], are rare gastric epithelio-mesenchymal biphasic tumors that occur in young adults. Granular SS, which tends to occur in older patients, has a sharp demarcation between spindle cell component and granular cells. This histologic feature differs from gastroblastoma's tendency to form epithelial clusters that often blend into the mesenchymal-like elements. *Sertoli-Leydig cell tumors*, a kind of sex cord–stromal tumor, are composed of variable proportions of Sertoli cells, Leydig cells, and a primitive gonadal stroma. The histologic appearance of epithelioid granular cells in our cases might be considered as luteinized cell-like and was similar to that of the Leydig cell component. In the case of intermediate or poorly differentiated Sertoli-Leydig cell tumors, Sertoli components also show spindle cell sarcoma–like features such that they have morphologic resemblance to spindle cells of SS. Even more confusing is that sex cord–stromal tumors are usually positive for inhibin-α regardless of histologic subtype [31]. Immunopositivity of the granular SS for inhibin-α could be a potential diagnostic pitfall. The spindle component in our cases, however, was negative for inhibin-α, whereas spindle cells of the Sertoli component are at least weakly positive. Immunoreactivity for hormonal receptors (estrogen receptor and progesterone receptor) of Sertoli-Leydig cell tumors also differs from that of granular SS. Immunopositivities for calretinin and WT1, for which most Sertoli-Leydig cell tumors are positive [32], might also be confusing, but it should be noted that SS cannot be ruled out by these immunohistochemical markers because calretinin positivity is recognized in a certain number of SS [22], and WT1-positive SS might not be rare (as we show in this study). Immunohistochemical differential diagnoses in soft tissue sarcoma might include *granular cell tumors* (inhibin-α positive) [33], but they are different from granular SS in that they rarely appear as biphasic histology and that they are usually positive for S100 protein. Despite the differential diagnoses above, a chromosomal translocation t(X;18) and resulting chimeric *SS18-SSX* gene have been shown to be characteristic of SS, and *SS18-SSX1* or *SS18-SSX2* fusion transcripts are identified in most SS cases [34,35]. The diagnoses of SS in the present cases were supported by demonstrating *SS18-SSX1* transcripts by RT-PCR analysis. Moreover, *SS18* rearrangements were confirmed in epithelioid granular cells and spindle tumor cells by dc-CISH.

In this study, we have described 2 cases of SS with granular cell features, occurring in older female subjects and showing immunoreactivity for inhibin-α and synaptophysin. These immunohistochemical findings have not been previously reported in SS and might be characteristic of granular SS. Their histologic and immunohistochemical features are potential diagnostic pitfalls. It is hoped that their cytologic

differentiation and biologic behavior will be clarified by further reports.

Acknowledgments

The authors have no conflict of interest to disclose. In addition, the authors thank Kyohei Yugawa for his excellent technical assistance.

References

[1] Drozenova J, Povysil C, Tvrdik D, Babjuk M, Hanus T. Primary synovial sarcoma of the kidney. Cesk Patol 2008;44:20-2.
[2] Argani P, Faria PA, Epstein JI, et al. Primary renal synovial sarcoma: molecular and morphologic delineation of an entity previously included among embryonal sarcomas of the kidney. Am J Surg Pathol 2000;24:1087-96.
[3] Kim DH, Sohn JH, Lee MC, et al. Primary synovial sarcoma of the kidney. Am J Surg Pathol 2000;24:1097-104.
[4] Fritsch M, Epstein JI, Perlman EJ, Watts JC, Argani P. Molecularly confirmed primary prostatic synovial sarcoma. Hum Pathol 2000;31: 246-50.
[5] Mitsuhashi A, Nagai Y, Suzuka K, et al. Primary synovial sarcoma in fallopian tube: case report and literature review. Int J Gynecol Pathol 2007;26:34-7.
[6] Nielsen GP, Shaw PA, Rosenberg AE, Dickersin GR, Young RH, Scully RE. Synovial sarcoma of the vulva: a report of two cases. Mod Pathol 1996;9:970-4.
[7] Chatzipantelis P, Kafiri G. Retroperitoneal synovial sarcoma: a clinicopathological study of 6 cases. J BUON 2008;13:211-6.
[8] Fisher C, Folpe AL, Hashimoto H, Weiss SW. Intra-abdominal synovial sarcoma: a clinicopathological study. Histopathology 2004; 45:245-53.
[9] Fisher C, de Bruijn DRH, Geurts van Kessel A. Synovial sarcoma. In: Fletcher CD, et al, editor. World Health Organization classification of tumours. Pathology and genetics of tumours of soft tissue and bone. Lyon, France: IARC Press; 2002. p. 200-4.
[10] Jin L, Majerus J, Oliveira A, et al. Detection of fusion gene transcripts in fresh-frozen and formalin-fixed paraffin-embedded tissue sections of soft-tissue sarcomas after laser capture microdissection and rt-PCR. Diagn Mol Pathol 2003;12:224-30.
[11] Motoi T, Kumagai A, Tsuji K, Imamura T, Fukusato T. Diagnostic utility of dual-color break-apart chromogenic in situ hybridization for the detection of rearranged SS18 in formalin-fixed, paraffin-embedded synovial sarcoma. Hum Pathol 2010;41:1397-404.
[12] Kumagai A, Motoi T, Tsuji K, Imamura T, Fukusato T. Detection of SYT and EWS gene rearrangements by dual-color break-apart CISH in liquid-based cytology samples of synovial sarcoma and Ewing sarcoma/ primitive neuroectodermal tumor. Am J Clin Pathol 2010;134:323-31.
[13] Meis-Kindblom JM, Stenman G, Kindblom LG. Differential diagnosis of small round cell tumors. Semin Diagn Pathol 1996;13:213-41.
[14] Milchgrub S, Ghandur-Mnaymneh L, Dorfman HD, Albores-Saavedra J. Synovial sarcoma with extensive osteoid and bone formation. Am J Surg Pathol 1993;17:357-63.
[15] Hisaoka M, Matsuyama A, Shimajiri S, et al. Ossifying synovial sarcoma. Pathol Res Pract 2009;205:195-8.
[16] Chan JA, McMenamin ME, Fletcher CD. Synovial sarcoma in older patients: clinicopathological analysis of 32 cases with emphasis on unusual histological features. Histopathology 2003;43:72-83.
[17] Povysil C. Synovial sarcoma with squamous metaplasia. Ultrastruct Pathol 1984;7:207-13.
[18] Krane JF, Bertoni F, Fletcher CD. Myxoid synovial sarcoma: an underappreciated morphologic subset. Mod Pathol 1999;12:456-62.
[19] van de Rijn M, Barr FG, Xiong QB, Hedges M, Shipley J, Fisher C. Poorly differentiated synovial sarcoma: an analysis of clinical, pathologic, and molecular genetic features. Am J Surg Pathol 1999; 23:106-12.
[20] Smith TA, Machen SK, Fisher C, Goldblum JR. Usefulness of cytokeratin subsets for distinguishing monophasic synovial sarcoma from malignant peripheral nerve sheath tumor. Am J Clin Pathol 1999; 112:641-8.
[21] Miettinen M, Limon J, Niezabitowski A, Lasota J. Patterns of keratin polypeptides in 110 biphasic, monophasic, and poorly differentiated synovial sarcomas. Virchows Arch 2000;437:275-83.
[22] Miettinen M, Limon J, Niezabitowski A, Lasota J. Calretinin and other mesothelioma markers in synovial sarcoma: analysis of antigenic similarities and differences with malignant mesothelioma. Am J Surg Pathol 2001;25:610-7.
[23] Olsen SH, Thomas DG, Lucas DR. Cluster analysis of immunohistochemical profiles in synovial sarcoma, malignant peripheral nerve sheath tumor, and Ewing sarcoma. Mod Pathol 2006;19:659-68.
[24] Tsuta K, Kato Y, Tochigi N, et al. Comparison of different clones (WT49 versus 6F-H2) of WT-1 antibodies for immunohistochemical diagnosis of malignant pleural mesothelioma. Appl Immunohistochem Mol Morphol 2009;17:126-30.
[25] Schraith DF, Hahm GK, Niemann TH, DeYoung BR. Alpha-inhibin immunoreactivity in soft-tissue neoplasia. Mod Pathol 2003;16: 1205-9.
[26] Leung PH, Salamonsen LA, Findlay JK. Immunolocalization of inhibin and activin subunits in human endometrium across the menstrual cycle. Hum Reprod 1998;13:3469-77.
[27] Miettinen M, Dow N, Lasota J, Sobin LH. A distinctive novel epitheliomesenchymal biphasic tumor of the stomach in young adults (gastroblastoma): a series of 3 cases. Am J Surg Pathol 2009;33: 1370-7.
[28] Matsuyama A, Hisaoka M, Iwasaki M, Iwashita M, Hisanaga S, Hashimoto H. TLE1 expression in malignant mesothelioma. Virchows Arch 2010;457:577-83.
[29] Butnor KJ, Nicholson AG, Allred DC, et al. Expression of renal cell carcinoma–associated markers erythropoietin, CD10, and renal cell carcinoma marker in diffuse malignant mesothelioma and metastatic renal cell carcinoma. Arch Pathol Lab Med 2006;130:823-7.
[30] Ordonez NG. The diagnostic utility of immunohistochemistry in distinguishing between mesothelioma and renal cell carcinoma: a comparative study. Hum Pathol 2004;35:697-710.
[31] Zhao C, Vinh TN, McManus K, Dabbs D, Barner R, Vang R. Identification of the most sensitive and robust immunohistochemical markers in different categories of ovarian sex cord–stromal tumors. Am J Surg Pathol 2009;33:354-66.
[32] Deavers MT, Malpica A, Liu J, Broaddus R, Silva EG. Ovarian sex cord–stromal tumors: an immunohistochemical study including a comparison of calretinin and inhibin. Mod Pathol 2003;16: 584-90.
[33] Le BH, Boyer PJ, Lewis JE, Kapadia SB. Granular cell tumor: immunohistochemical assessment of inhibin-alpha, protein gene product 9.5, S100 protein, CD68, and Ki-67 proliferative index with clinical correlation. Arch Pathol Lab Med 2004;128:771-5.
[34] Crew AJ, Clark J, Fisher C, et al. Fusion of SYT to two genes, SSX1 and SSX2, encoding proteins with homology to the Kruppel-associated box in human synovial sarcoma. EMBO J 1995;14: 2333-40.
[35] Fligman I, Lonardo F, Jhanwar SC, Gerald WL, Woodruff J, Ladanyi M. Molecular diagnosis of synovial sarcoma and characterization of a variant SYT-SSX2 fusion transcript. Am J Pathol 1995;147:1592-9.

Variation in myxoid liposarcoma: Clinicopathological examination of four cases with detectable *TLS-CHOP* or *EWS-CHOP* fusion transcripts whose histopathological diagnosis was other than myxoid liposarcoma

KAYO SUZUKI[1], YOSHITO MATSUI[1], NOBUYUKI HASHIMOTO[2], NORIFUMI NAKA[2], NOBUHITO ARAKI[3], TOMOATSU KIMURA[1], HIDEKI YOSHIKAWA[2] and TAKAFUMI UEDA[4]

[1]Department of Orthopaedic Surgery, University of Toyama, Toyama 930-0194;
[2]Department of Orthopaedics, Osaka University Graduate School of Medicine, Suita, Osaka 565-0871;
[3]Department of Orthopaedic Surgery, Osaka Medical Center for Cancer and Cardiovascular Diseases, Osaka 537-8511;
[4]Department of Orthopaedic Surgery, Osaka National Hospital, Osaka 540-0006, Japan

Received July 18, 2011; Accepted October 11, 2011

DOI: 10.3892/ol.2011.480

Abstract. Liposarcomas are separated into clinicopathological entities by a characteristic morphological spectrum and distinctive genetic changes. Myxoid liposarcoma (MLS) represents one such entity with specific chromosomal translocations leading to the generation of fusion genes, the human translocation liposarcoma (*TLS*)-CCAAT/enhancer binding protein (*C/EBP*) homologous protein (*CHOP*) or the Ewing sarcoma (*EWS*)-*CHOP*. In the present study, four cases of liposarcoma with detection of *TLS-CHOP* or *EWS-CHOP*, whose postoperative diagnosis was other than MLS (one well-differentiated liposarcoma, two de-differentiated liposarcomas and one unclassified) were examined for medical records, imaging data and histopathology. Clinical records demonstrated that three of the four cases were considerably difficult to diagnose definitively, and histopathological re-examination pointed out areas of myxomatous change as a minor component (<10%). Their dominant components (>90%) resembled pleomorphic sarcoma, pleomorphic malignant fibrous histiocytoma and monophasic synovial sarcoma. The current cases may represent an extreme variant of the morphological spectrum within MLS. In cases of difficulty in making definitive diagnosis of soft tissue sarcoma by standard histopathological examination and identification of myxoid stroma even as a minor component, analyzing *TLS-CHOP* and *EWS-CHOP* fusion genes may aid the diagnosis of unusual MLS.

Correspondence to: Dr Yoshito Matsui, Department of Orthopaedic Surgery, University of Toyama, 2630 Sugitani, Toyama 930-0194, Japan
E-mail: m-yoshito@umin.ac.jp

Key words: Ewing sarcoma-CCAAT/enhancer binding homologous protein, histopathology, myxoid liposarcoma, reverse transcription-polymerase chain reaction, human translocation liposarcoma-CCAAT/enhancer binding homologous protein, variation

Introduction

Liposarcomas are the most common class of soft tissue sarcoma, and are separated into distinct clinicopathological entities with a characteristic morphological spectrum and exclusive genetic changes (1,2). Myxoid liposarcoma (MLS) represents one such entity with the second most common prevalence after well-differentiated liposarcoma. A significant proportion of MLS contains a cytogenetic hallmark, t(12;16)(q13;p11), which leads to the fusion of the CCAAT/enhancer binding protein (*C/EBP*) homologous protein (*CHOP*) and human translocation liposarcoma (*TLS*) gene, generating *TLS-CHOP* fusion transcript (3-10). In a minor population of MLS, a variant chromosomal translocation, t(12;22)(q13;q12), has been documented, resulting in the Ewing sarcoma (*EWS*)-*CHOP* fusion gene (5,6,8-12). Our recent fusion gene analysis of 172 cases of adipocytic tumors, comprising 98 cases of lipoma and 74 cases of liposarcoma, established that *TLS-CHOP* and *EWS-CHOP* were specific to liposarcoma (10). However, of note, among the distinct entities of liposarcomas, the fusion genes were detectable in four cases whose histopathological diagnosis was other than MLS. The present study aimed to re-examine the clinicopathological features of these four 'unusual' cases, and the results indicated the histopathological variation in MLS.

Materials and methods

Case selection. The patients included in this study were 2 males and 2 females, ranging in age from 32 to 74 years (mean 59), who presented with a mass lesion ranging from 2.5 to 14 cm in size. After written informed consent was obtained, tissues from 74 liposarcomas obtained at the time of surgery, and stored at -80°C, were analyzed by reverse transcription-polymerase chain reaction (RT-PCR) and DNA sequencing

Table I. Clinicopathological characteristics of four cases with detectable *TLS-CHOP* or *EWS-CHOP* transcripts whose diagnosis was other than myxoid liposarcoma.

No.	Age/ Gender	Location	Size (cm)	Postoperative diagnosis	Differential diagnosis and dominant cells	Myxomatous component	Adjuvant therapy	Follow-up after wide resection	Fusion gene
1	70/M	Thigh	>10	WDLS	ND	ND	No	72 mo ANED	*TLS-CHOP*
2	74/F	Thigh	2.5	DDLS	Pleomorphic sarcoma, spindle cells	<10%	No	129 mo ANED	*TLS-CHOP*
3	58/M	Retro-peritoneum	ND	DDLS	Pleomorphic MFH, spindle cells	<10%	Chemo, Radio	22 mo rec; 40 mo SD	*EWS-CHOP*
4	32/F	Back	14	Unclassified	Synovial sarcoma, spindle cells	<5%	Chemo	36 mo ANED, DID	*TLS-CHOP*

ANED, alive no evidence of disease; DDLS, de-differentiated liposarcoma; DID, deceased independent of disease; SD, succumbed to disease; F, female; M, male; MFH, malignant fibrous histiocytoma; mo, months; ND, no data; rec, local recurrence; WDLS, well-differentiated liposarcoma; Chemo, chemotherapy; Radio, radiotherapy.

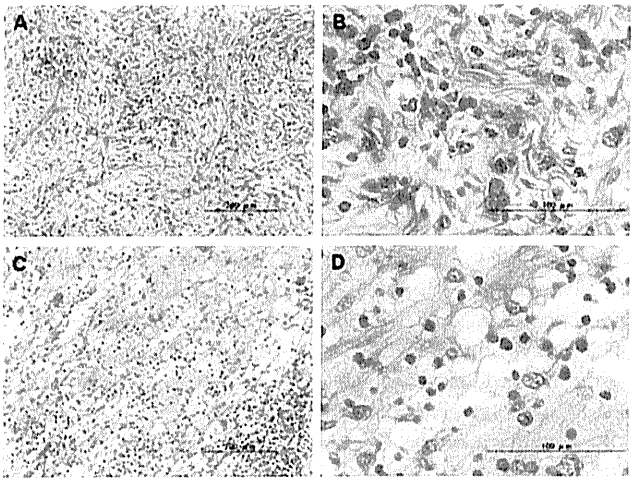

Figure 1. Histopathological re-examination of the biopsy specimen (case 2). (A) The dominant component (>90%) showed variable cellularity and cytological pleomorphism with collagenous matrix, an appearance of pleomorphic sarcoma (magnification, x100). (B) High-power magnification of the dominant component contained large bizarre cells with foamy cytoplasm (magnification, x400). (C) The minor component (<10%) contained abundant intercellular myxoid stroma with notable infiltration of inflammatory cells (magnification, x100). (D) High-power magnification of the minor component (magnification, x400). Hematoxylin and eosin staining.

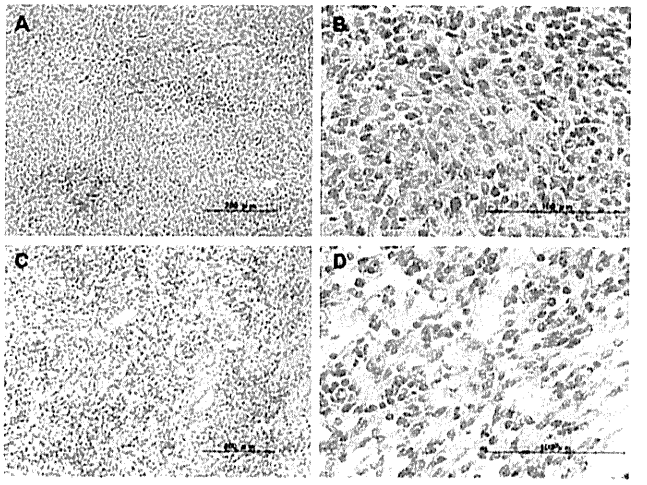

Figure 2. Histopathological re-examination of the biopsy specimen (case 4). (A) The dominant component (>95%) consisted of fascicles and sheets of uniform, relatively small ovoid neoplastic cells, mimicking typical appearance of monophasic synovial sarcoma (magnification, x100). (B) High-power magnification of the dominant component (magnification, x400). (C) The minor component (<5%) contained small amount of intercellular myxoid stroma and neoplastic cells were not closely packed (magnification, x100). (D) High-power magnification of the minor component (magnification, x400). Hematoxylin and eosin staining.

for possible detection of the *TLS-CHOP* or *EWS-CHOP* transcripts (10). Histological subtypes of liposarcomas, determined by pathologists, consisted of 12 well-differentiated, 41 MLS, 4 de-differentiated, and 17 unclassified. Out of the 74 liposarcomas, 22 (30%) were associated with the *TLS-CHOP* fusion transcript, whereas 3 (4%) were associated with the *EWS-CHOP* fusion transcript. Histological subtypes of *TLS-CHOP* detection consisted of 1 well-differentiated (8% of the subtype), 19 MLS (46% of the subtype), 1 de-differentiated (25% of the subtype) and 1 unclassified (6% of the subtype). Histological subtypes of *EWS-CHOP* detection in liposarcoma included 2 MLS (2% of the subtype) and 1 de-differentiated (25% of the subtype). Based on the above, four cases of liposarcoma with detection of either *TLS-CHOP* or *EWS-CHOP* whose postoperative diagnosis was other than MLS were selected for the current study, consisting of re-examination of medical records, imaging data and histopathology. The procurement of frozen tissues and retrospective data collection were approved by the Review Boards of Osaka University Hospital and Osaka Medical Center for Cancer and Cardiovascular Diseases.

Results

Clinically, the patients were 2 male and 2 female, ranging in age from 32 to 74 (mean 59) years, and presenting with a mass lesion ranging from 2.5 to 14 cm in size (Table I).

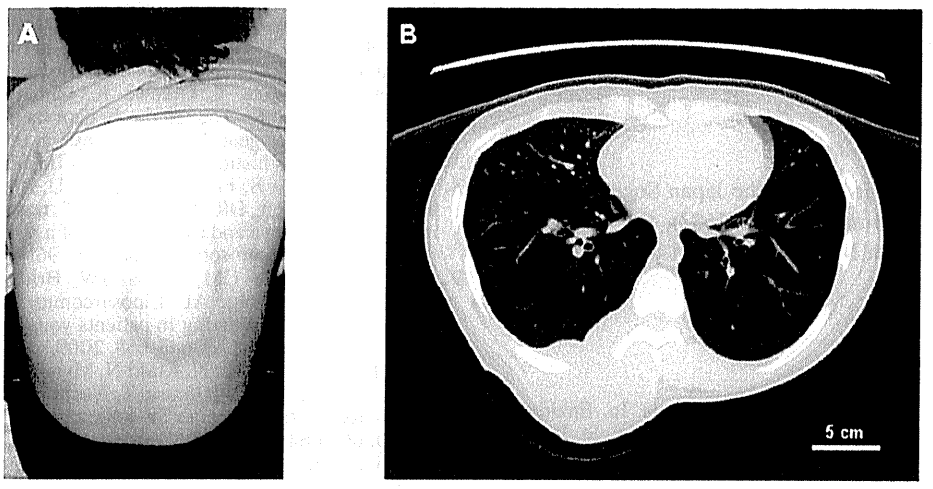

Figure 3. (A) Clinical image of case 4. A large mass located in the right section of the back. (B) Computed tomography image demonstrating the lesion mostly localized in the back muscle, partly penetrating into the thorax.

Postoperative diagnoses were well-differentiated liposarcoma (case 1), de-differentiated liposarcoma (cases 2 and 3), and unclassified (case 4). The patients underwent wide-resection with or without adjuvant therapy. Follow-up was available for all 4 patients and ranged from 36 to 129 months (mean 69) after surgery.

Re-examination of the clinical records identified that three of the four cases (cases 2, 3 and 4 in Table I) experienced considerable difficulty in making definitive diagnosis. Histopathologically, two cases postoperatively diagnosed as de-differentiated liposarcoma (cases 2 and 3 in Table I) exhibited variable cellularity and cytological pleomorphism, and contained large bizarre cells with foamy cytoplasm (Fig. 1A and 1B). In one case postoperatively diagnosed as unclassified (case 4 in Table I), spindle cells were densely proliferated (Fig. 2A and B); however, the tentative diagnosis of monophasic synovial sarcoma was postulated by the subsequent RT-PCR analysis, which did not detect any synovial sarcoma, translocated to X chromosome (*SYT*)-sarcoma, synovial, X breakpoint (*SSX*) fusion transcripts for the definitive diagnosis (13). Re-examination of the histopathology identified that these three cases contained areas of myxomatous change as a minor component (<10%) (Figs. 1C and D and 2C and D).

Clinical report (case 4). A 32-year-old female presented with a large mass measuring 14 cm located on her back (Fig. 3A), which had occasional pain from one month prior to presentation. Computed tomography demonstrated that the mass lesion was predominantly located under the fascia of the back muscle, but partly penetrated into the thorax (Fig. 3B). Magnetic resonance imaging revealed non-homogeneous enhancement of the lesion following gadolinium diethylenetriaminepentaacetic acid injection. Open biopsy clearly supported the malignant nature of the lesion (Fig. 2A and B), and wide-resection was achieved with adjuvant pre- and post-operative chemotherapy. There were no signs of recurrence or metastasis prior to the patient's death due to suicide at 36 months after surgery.

Discussion

According to the World Health Organization (WHO) classification, MLS is defined as 'a malignant tumor composed of uniform round to oval-shaped primitive non-lipogenic mesenchymal cells and a variable number of lipoblasts in a prominent myxoid stroma with a characteristic branching vascular pattern' (2). In this retrospective analysis of four cases, their postoperative diagnoses, divided into various classes, were revised to MLS following the detection of the *TLS-CHOP* or *EWS-CHOP* fusion transcripts. With the exception of one case (case 1) whose histopathological material was not available, re-examination proved that these cases shared a common characteristic, i.e., a myxomatous area as a minor component (<10%), indicating that there are unusual MLS cases whose myxoid stroma is not prominent.

Dominant components (>90%) of the current cases resembled pleomorphic sarcoma (case 2), pleomorphic malignant fibrous histiocytoma (case 3) and monophasic synovial sarcoma (case 4). In cases 2 and 3, the dominant component had been regarded as a de-differentiated feature of the de-differentiated liposarcoma. As shown in mixed-type liposarcomas consisting of combined patterns of well-differentiated liposarcoma and MLS, these cases (and possibly also case 1) may represent an extreme variant of the morphological spectrum within MLS (14). On the other hand, in case 4, the contradiction between histopathological appearance and the negative detection of *SYT-SSX* fusion transcripts resulted in a delay in classification, and this case was considered to comprise exclusively round-cell type MLS.

In conclusion, the present study indicates the histopathological variation in MLS and the significance of fusion gene detection for definitive diagnosis. In case of i) difficulty in providing definitive diagnosis of soft tissue sarcoma by standard histopathological examination; ii) negative detection of the histopathological candidate fusion gene (as in case 4 in this study); and iii) recognition of myxoid stroma even as a minor component, we propose that analysis of *TLS-CHOP* and *EWS-CHOP* fusion genes may aid diagnosis of unusual

MLS. Further studies on the correlation between fusion genes and clinicopathological characteristics of MLS are required to establish the specific identity of this class.

Acknowledgements

This study was supported in part by the Japan Society for the Promotion of Science (Grant no. 22591683), the Nakatomi Foundation and the Osaka Medical Research Foundation for Incurable Diseases.

References

1. Weiss SW and Goldblum JR (eds): Liposarcoma. In: Enzinger and Weiss's Soft Tissue Tumors, 4th edition. Mosby, St. Louis, pp641-93, 2001.
2. Antonescu CR and Ladanyi M: Myxoid liposarcoma. In: World Health Organization Classification of Tumours: Pathology and Genetics of Tumours of Soft Tissue and Bone. Fletcher CDM, Unni KK and Mertens F (eds). IARC Press, Lyon, pp40-43, 2002.
3. Antonescu CR, Elahi A, Humphrey M, Lui MY, Healey JH, Brennan MF, Woodruff JM, Jhanwar SC and Ladanyi M: Specificity of *TLS-CHOP* rearrangement for classic myxoid/round cell liposarcoma: absence in predominantly myxoid well-differentiated liposarcomas. J Mol Diagn 2: 132-138, 2000.
4. Panagopoulos I, Mertens F, Isaksson M and Mandahl N: A novel *FUS/CHOP* chimera in myxoid liposarcoma. Biochem Biophys Res Commun 279: 838-845, 2000.
5. Antonescu CR, Tschernyavsky SJ, Decuseara R, Leung DH, Woodruff JM, Brennan MF, Bridge JA, Neff JR, Goldblum JR and Ladanyi M: Prognostic impact of P53 status, *TLS-CHOP* fusion transcript structure, and histological grade in myxoid liposarcoma: a molecular and clinicopathologic study of 82 cases. Clin Cancer Res 7: 3977-3987, 2001.
6. Hosaka T, Nakashima Y, Kusuzaki K, Murata H, Nakayama T, Nakamata T, Aoyama T, Okamoto T, Nishijo K, Araki N, *et al*: A novel type of *EWS-CHOP* fusion gene in two cases of myxoid liposarcoma. J Mol Diagn 4: 164-171, 2002.
7. Domoto H, Hosaka T, Oikawa K, Ohbayashi T, Ishida T, Izumi M, Iwaya K, Toguchida J, Kuroda M and Mukai K: *TLS-CHOP* target gene *DOL54* expression in liposarcomas and malignant fibrous histiocytomas. Pathol Int 52: 497-500, 2002.
8. Bode-Lesniewska B, Frigerio S, Exner U, Abdou MT, Moch H and Zimmermann DR: Relevance of translocation type in myxoid liposarcoma and identification of a novel *EWSR1-DDIT3* fusion. Genes Chromosomes Cancer 46: 961-971, 2007.
9. Alaggio R, Coffin CM, Weiss SW, Bridge JA, Issakov J, Oliveira AM and Folpe AL: Liposarcomas in young patients: a study of 82 cases occurring in patients younger than 22 years of age. Am J Surg Pathol 33: 645-658, 2009.
10. Kubo T, Matsui Y, Naka N, Araki N, Myoui A, Endo K, Yasui N, Ohtani O, Suzuki K, Kimura T, Yoshikawa H and Ueda T: Specificity of fusion genes in adipocytic tumors. Anticancer Res 30: 661-664, 2010.
11. Matsui Y, Ueda T, Kubo T, Hasegawa T, Tomita Y, Okamoto M, Myoui A, Kakunaga S, Yasui N and Yoshikawa H: A novel type of *EWS-CHOP* fusion gene in myxoid liposarcoma. Biochem Biophys Res Commun 348: 437-440, 2006.
12. Suzuki K, Matsui Y, Endo K, Kubo T, Hasegawa T, Kimura T, Ohtani O and Yasui N: Myxoid liposarcoma with *EWS-CHOP* type 1 fusion gene. Anticancer Res 30: 4679-4684, 2010.
13. Ladanyi M, Antonescu CR, Leung DH, Woodruff JM, Kawai A, Healey JH, Brennan MF, Bridge JA, Neff JR, Barr FG, *et al*: Impact of *SYT-SSX* fusion type on the clinical behavior of synovial sarcoma: a multi-institutional retrospective study of 243 patients. Cancer Res 62: 135-140, 2002.
14. De Vreeze RSA, De Jong D, Koops W, Nederlof PM, Ariaens A, Haas RL and van Coevorden F: Oncogenesis and classification of mixed-type liposarcoma: a radiological, histopathological and molecular biological analysis. Int J Cancer 128: 778-786, 2011.

The Foot 21 (2011) 157–161

Contents lists available at ScienceDirect

The Foot

journal homepage: www.elsevier.com/locate/foot

Case report

Prosthetic reconstruction for tumors of the distal tibia. Report of two cases

Kenichiro Hamada*, Norifumi Naka, Yoichi Murata, Yukihiko Yasui, Susumu Joyama, Nobuhito Araki

Department of Orthopaedic Surgery, Osaka Medical Center for Cancer and Cardiovascular Diseases, 1-3-3, Nakamichi, Higashinari-ku, Osaka, 537-8511, Japan

ARTICLE INFO

Article history:
Received 16 September 2010
Received in revised form 20 January 2011
Accepted 20 January 2011

Keywords:
Malignant bone tumor
Distal tibia
Custom made prosthesis

ABSTRACT

Prosthetic reconstruction in two patients with malignant bone tumors of the distal tibia was conducted. The diagnoses were metastatic bone tumor in one patient and low grade central osteosarcoma in another. The mean duration of follow-up was 5.5 years (3 and 8 years). Reconstruction was achieved using custom-made prosthesis (JMM, Japan Medical Materials), which replaced the distal tibia. In the patient with metastasis, local recurrence occurred 8 months after the primary surgery and the recurrent tumor was resected. Both patients were free from neoplastic disease at the latest follow-up. The average functional scores according to the system of the Musculoskeletal Tumor Society were 25 and 23. Custom-made prostheses allow an early return to functional weight-bearing without major complications. This technique provides a safe and effective method of stabilization for properly selected malignant tumors of the distal tibia.

© 2011 Elsevier Ltd. All rights reserved.

1. Introduction

Malignant bone tumors of the distal tibia are very rare [1]. Below knee amputation has been a surgical treatment of choice for the local tumor with satisfactory functional results [1,2]. The subcutaneous location and proximity of the distal tibia to the neurovascular bundle and tendons make adequate excision with wide margins of malignant tumors of the distal tibia difficult to achieve [2]. Therefore, there have been only few publications on prosthetic replacement of the distal tibia [1,2].

In this study, custom-made prosthetic reconstruction without talar surface replacement in two patients with malignant tumors of the distal tibia was performed. Hence, the clinical and functional results of this method are being presented.

2. Preoperative planning and custom-made prosthesis

Before operation, the patients were assessed to determine the extent of the local disease and presence of metastases by clinical assessment, plain radiography, and chest tomography (CT). Magnetic resonance imaging (MRI) was also performed to define the extent of the tumor, involvement of the soft tissues, particularly the neurovascular bundle, and level of bone resection.

The prosthetic system (Japan Medical Materials Ltd., Kyoto, Japan) is custom-made based on the anticipated level of resection of tibia for distal tibial bone tumors (Fig. 1). The prosthesis takes approximately 6 weeks to prepare.

3. Operative technique

Surgical approach was determined by the position of the tumor. Meticulous resection was carried out to possibly preserve a wide margin of tissue. The tumor was excised en-bloc (Fig. 2A and B). The proximal intramedullary canal was reamed and the stem was secured with bone cement, with a clinical outcome of appropriate rotational alignment in mind (Fig. 2C). The joint elements made with ultrahigh molecular weight polyethylene (UMWP) were manufactured to fit the talar joint surface. The range of motion and stability of the ankle were evaluated before the skin was closed.

4. Post operative rehabilitation

The patient was mobilized from bed to chair within the first 48 h postoperatively. A short-leg splint was applied after four weeks and then passive and active movements were commenced (Fig. 2D). Partial weight-bearing was allowed at 4 weeks, which progressed to full weight-bearing at about 6 weeks.

5. Functional assessment

Functional outcome was assessed using the Musculoskeletal Tumor Society (MSTS) functional evaluation system [3]. The MSTS score is composed of pain, function, emotional acceptance, walking ability, gait, and use of walking aids, with a higher score indicating better functional outcome.

* Corresponding author. Tel.: +81 6 6879 1181.
E-mail address: hamada-ke@mc.pref.osaka.jp (K. Hamada).

0958-2592/$ – see front matter © 2011 Elsevier Ltd. All rights reserved.
doi:10.1016/j.foot.2011.01.014